GUIDANCE AND NAVIGATION FOR RENDEZVOUS AND PROXIMITY OPERATIONS WITH A NON–COOPERATIVE SPACECRAFT AT GEOSYNCHRONOUS ORBIT

Brent Wm. Barbee[*], J. Russell Carpenter[†], Scott Heatwole[‡], F. Landis Markley[§], Michael Moreau[†], Bo J. Naasz[†], and John Van Eepoel[§]

The feasibility and benefits of various spacecraft servicing concepts are currently being assessed, and all require that the servicer spacecraft perform rendezvous, proximity, and capture operations with the target spacecraft to be serviced. Many high-value spacecraft, which would be logical targets for servicing from an economic point of view, are located in geosynchronous orbit, a regime in which autonomous rendezvous and capture operations are not commonplace. Furthermore, existing GEO spacecraft were not designed to be serviced. Most do not have cooperative relative navigation sensors or docking features, and some servicing applications, such as de-orbiting of a non-functional spacecraft, entail rendezvous and capture with a spacecraft that may be non-functional or un-controlled. Several of these challenges have been explored via the design of a notional mission in which a non-functional satellite in geosynchronous orbit is captured by a servicer spacecraft and boosted into super-synchronous orbit for safe disposal. A strategy for autonomous rendezvous, proximity operations, and capture is developed, and the Orbit Determination Toolbox (ODTBX) is used to perform a relative navigation simulation to assess the feasibility of performing the rendezvous using a combination of angles-only and range measurements. Additionally, a method for designing efficient orbital rendezvous sequences for multiple target spacecraft is utilized to examine the capabilities of a servicer spacecraft to service multiple targets during the course of a single mission.

INTRODUCTION

The National Aeronautics and Space Administration (NASA) has undertaken a study to assess the feasibility, practicality, and cost of servicing satellites using elements of currently planned and future NASA human spaceflight systems and/or robotic spacecraft technologies. Spacecraft servicing can have several motivations, from extending the life of unique, high value assets such as the Hubble Space Telescope, to disposal of dead spacecraft or orbital debris that pose a hazard to other spacecraft or the public, to the repairing or refueling of commercial satellites as a more economical alternative to replacement. Moreover, the technologies that enable this sort of spacecraft servicing could then be directly applied to large-scale future missions, such as the on-orbit assembly of large telescopes.

One area that has received some attention in the servicing study is applications to spacecraft in geostationary (GEO) orbits. While servicing can benefit spacecraft in a variety of orbital regimes, many of the highest value spacecraft inhabit GEO (e.g., communications, Earth observation). Designing, fabricating, and launching spacecraft into GEO is extremely expensive and it would thus be highly desirable to spacecraft operators to extend the lifetimes of their existing GEO spacecraft rather than replace them. Furthermore, GEO spacecraft that have irrevocably failed before proper disposal will drift through the GEO belt and pose a collision hazard to crucial spacecraft assets; it would therefore be of great value for a servicer spacecraft to boost such non-functional spacecraft into a proper disposal orbit. A servicing spacecraft deployed to GEO could conceivably service multiple spacecraft since there would be multiple potential target spacecraft with similar

[*]Aerospace Engineer, Emergent Space Technologies, Inc., 6301 Ivy Lane, Suite 720, Greenbelt, MD 20770, USA.
[†]Aerospace Engineer, NASA Goddard Space Flight Center, Code 595, 8800 Greenbelt Road, Greenbelt, MD 20771, USA.
[‡]Aerospace Engineer, NASA GSFC's Wallops Flight Facility, Code 598, Rt. 175, Wallops Island, VA 23337, USA.
[§]Aerospace Engineer, NASA Goddard Space Flight Center, Code 591, 8800 Greenbelt Road, Greenbelt, MD 20771, USA.

semimajor axes and orbit planes. For these reasons, performing servicing at GEO could be cost-effective for spacecraft operators, and even has the potential of being operated as a commercial-for-profit venture.

Successful servicing requires the synthesis and advancement of the current state of the art technologies and capabilities in the areas of space robotics, vehicle-relative navigation sensors, spacecraft Guidance, Navigation, and Control (GN&C) algorithms, and spacecraft autonomy. In this paper we explore some of the specific challenges associated with guidance, navigation, rendezvous, and proximity operations with a non-cooperative target spacecraft in GEO.

Autonomous Rendezvous, Proximity Operations, and Capture (AR&C) Challenges

AR&C has historically not been commonplace in GEO, and is challenging for a variety of reasons. AR&C systems tend to be designed for operations in LEO, but GEO presents a different environment for the sensors and algorithms to cope with. The significantly higher altitude at GEO means that the dominant dynamics are much slower, making the characteristic distance and time scales for rendezvous different than in LEO. This can impact relative navigation filter design and performance. Spacecraft hardware is exposed to more radiation and will require additional shielding. The Global Positioning System (GPS) satellite constellation is far below the spacecraft, requiring weak-signal GPS tracking to obtain sufficient GPS measurements, which in turn requires advanced GPS receiver hardware and algorithms capable of fast acquisition and weak signal tracking.

The situation is further complicated when, as is the case for almost all existing GEO satellites in operation today, the target spacecraft to be captured and serviced is non-cooperative. For instance, they lack rendezvous aids such as retro-reflectors or other rendezvous sensor tracking features and they are not designed to exchange helpful telemetry with an approaching servicer (e.g., two-way radio frequency crosslink ranging). Many potential targets will not have docking or grapple fixtures designed specifically for capture, requiring use of a robotic arm to capture the spacecraft in an innovative manner. Finally, AR&C becomes more challenging when the target spacecraft is unable to act cooperatively with the servicer to facilitate rendezvous and capture; such would be the case for disposal of a non-functional spacecraft.

A worst case scenario is a completely non-cooperative target consisting of a non-functional spacecraft that is an uncontrolled attitude state, e.g., tumbling, and for which the only available absolute orbit determination consists of state vectors derived from ground station tracking. In such a case, the target spacecraft orbit may only be known to an accuracy of 10's or even 100's of km, the range of some relative navigation sensors could be limited, and the servicer spacecraft would be forced to match rates with the target during final approach and capture.

Notional Mission Scenario

The notional mission scenario selected for this paper is the disposal (to a super-synchronous graveyard orbit) of a non-functional, non-cooperative target spacecraft in GEO. Although this paper studies the general application of disposal of a GEO satellite, a recent, real-world example of such a target is DSP-23, an Earth-observing military satellite launched in November of 2007, which subsequently ceased operating during late 2008 for unknown reasons. DSP-23 is currently drifting through the GEO belt, posing a collision hazard to other spacecraft; amateur satellite observers have reported DSP-23 passing within < 12 km of operational GEO satellites*.

In our mission scenario a servicer spacecraft equipped with robotic arms and an AR&C sensor suite is launched and maneuvered into an orbit that is co-elliptic with the target spacecraft. The servicer then performs rendezvous and proximity operations with the target, culminating in the initiation of safety ellipse motion about the target. After inspecting the target during the safety ellipse motion (possibly for several days), the servicer begins moving down a capture axis toward the target until it is able to grapple the target using robotic arms. After the robotic arms are rigidized and the spacecraft stack (servicer and target) are firmly under the servicer's control, the servicer boosts itself and the target to a proper disposal orbit (approximately

*http://www.space.com/news/090225-wandering-spysat-danger.html

GEO altitude + 300 km), releases the target, and moves away safely. From there the servicer can continue super-synching targets until it has only enough fuel left to safely dispose of itself.

RENDEZVOUS STRATEGY

We assume that the launch vehicle upper stage, or maneuvers that are planned by ground operators following launch, will deliver the servicer spacecraft into an orbit that is co-elliptic with the target spacecraft's orbit, as shown in Figure 1. This will place the servicer spacecraft's orbit in the same plane as that of the target, with the same eccentricity and aligned apse lines*. The difference in semimajor axis between the orbits creates an altitude difference between the spacecraft that produces a desired relative drift between them. The servicer spacecraft can generally be above or below the target, but starting below may be considered safer as it does not require the servicer to cross the target's orbit prior to terminal rendezvous.† The servicer spacecraft will be moving faster than the target when below it, so to close distance requires that the servicer spacecraft begin AR&C operations at a point behind the target.

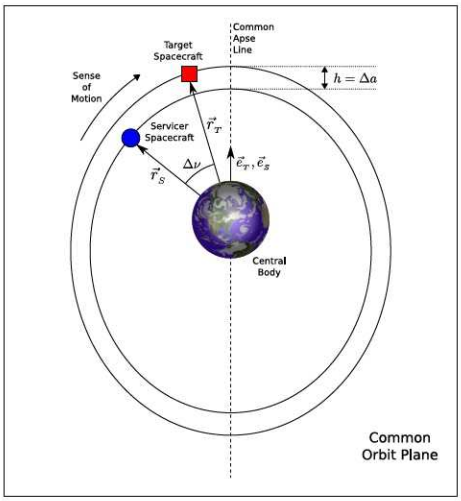

Figure 1. Co-Elliptic Orbits

Co-Elliptic Rendezvous Profile

The design of a rendezvous profile to take the servicer spacecraft from an initial co-elliptic orbit to insertion onto a safety ellipse in the proximity of the target spacecraft is shown in Figure 2. The servicer spacecraft is shown after having been inserted into a co-elliptic orbit with the target spacecraft. After some period of drifting, the servicer begins performing relative navigation with the target spacecraft.

The servicer begins 30 km below (h_1) and approximately 300 km behind (s_1) the target in the target's Radial, In-Track, Cross-Track (RIC) frame. The co-elliptic rendezvous sequence consists of 3 drift segments separated by 2 Hohmann raises. The servicer will continue to drift for a time interval Δt_1, after which it will perform the first of the Hohmann transfers. The first Hohmann raise increases the servicer's altitude by 25 km, bringing it to 5 km below the target (h_2) while still behind it. The second Hohmann raise increases the servicer's altitude once more by 4 km, bringing it to 1 km below the target (h_3) while still behind it. The servicer then drifts at 1 km below the target until the remaining In-Track distance is covered, bringing the servicer directly below the target, 1 km down. Once the In-Track separation between the servicer and the target becomes zero at the end of the final co-elliptic drift segment, proximity operations begin with the

*Generally the spacecraft orbits will be nearly, but not exactly, circular.

†Approach from below may also make optical sensing easier as Earth is less likely to be in the field of view of a camera or star tracker used for this purpose (although this may be less of an issue at GEO than at LEO–the angular size of Earth is smaller at GEO.)

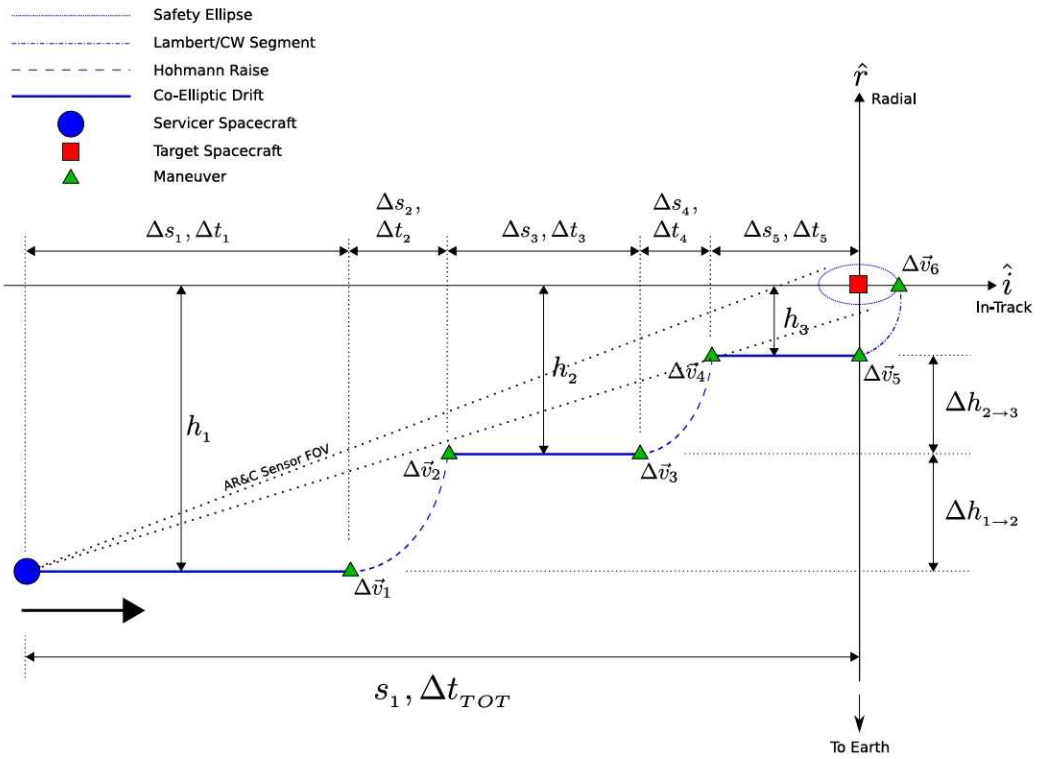

Figure 2. Co-Elliptic Rendezvous with Hohmann Raises Culminating in Safety Ellipse Insertion

servicer maneuvering onto a trajectory that will take it to the proper coordinates for safety ellipse insertion ahead of, and out of plane with, the target vehicle.

During co-elliptic drift segments the servicer spacecraft moves at a constant rate parallel to the In-Track direction towards the target. The rate of approach depends on the altitude difference, h, between the spacecraft. The In-Track distance covered while drifting at a given relative altitude for a given amount of time is given by

$$\Delta s = a_{TARG} \left| n_{TARG} - n_{SERV} \right| \Delta t \tag{1}$$

where a_{TARG} is the semimajor axis of the target spacecraft, n_{TARG} is the mean motion of the target spacecraft, n_{SERV} is the mean motion of the servicer spacecraft, and Δt is the amount of time spent drifting. Conversely, Eq. 1 may be solved for Δt in order to compute the amount of time required to cover a given amount of drift distance, Δs. The effect of the altitude difference between the spacecraft manifests in the difference between their mean motions (since mean motion is a function of the spacecraft semimajor axis and the altitude difference causes a corresponding difference in the semimajor axes of the spacecraft).

Table 1 presents the times elapsed and In-Track distances covered during each segment of the co-elliptic rendezvous. We choose co-elliptic coast arc durations of 36 hours, with the notion that allowing the navigation filter more than one orbit between maneuvers for convergence and settling would provide adequate state estimation performance. We choose an initial In-Track separation distance of approximately 300 km for the start of AR&C, a very conservative range at which bearing sensors could first acquire the sun-illuminated target. An initial altitude 30 km below the target is a reasonable choice for the final delivery orbit subsequent to launch and orbital maneuvering by the launch vehicle's upper stage (although a greater altitude difference may be useful in reducing the phasing time between launch and rendezvous or expanding the launch window– this altitude difference is a convenient place to start this analysis.)

Table 1. Co-Elliptic Rendezvous Segment Distances and Times

Segment	Description	Altitude Change (Δh), km	Distance (Δs), km	Time (Δt), hours
1	Co-Elliptic Drift	0	118.0988	10
2	Hohmann Raise	+25	82.4583	11.974
3	Co-Elliptic Drift	0	70.8068	36
4	Hohmann Raise	+4	14.1369	11.980
5	Co-Elliptic Drift	0	13.9176	36
Totals		**+29**	**299.4184**	**105.954**

We use Eq. 1, along with the standard Hohmann transfer equations, to structure the remaining parameters for the co-elliptic rendezvous sequence so as to provide a smooth profile. The total time elapsed during the co-elliptic rendezvous portion of AR&C is approximately 4.4 days, which should provide adequate time for ground control to monitor the approach and manage any events that require attention.

The magnitudes of the rendezvous maneuvers computed in the simulation are presented in Table 2. The magnitudes presented are the L^1 norms (sum of components) rather than the usual Euclidean norms in order to provide a conservative estimate of the required maneuver ΔV that accounts for the fact that the servicer spacecraft will not be able to simply orient itself such that it aligns a single thruster with the desired thrust direction to perform a particular maneuver. Rather, the servicer must maintain an attitude that continuously points its relative navigation sensors at the target spacecraft and will apply ΔV vectors by firing multiple thrusters pointing in different directions.

Table 2. Co-Elliptic Hohmann Raise Maneuver Magnitudes

Maneuver	L^1 Norm Magnitude (m/s)
Hohmann Raise Start, ΔV_1	0.622541
Hohmann Raise Stop, ΔV_2	0.622842
Hohmann Raise Start, ΔV_3	0.099069
Hohmann Raise Stop, ΔV_4	0.099186

The co-elliptic rendezvous approach has several important advantages. First, by varying the choice of initial In-Track separation, the choice of initial altitude difference, and the schedule of altitude raises, the timing and geometry of the rendezvous can be controlled within the limits of orbital mechanics. For instance, specific amounts of drift time between altitude raise maneuvers can be obtained, which may be useful for ensuring navigation filter convergence and accuracy, as described previously.

Second, the sequence of drifts and altitude raises grants a measure of passive collision avoidance safety to the relative motion because if the servicer loses the ability to maneuver at any time, or chooses to not complete the rendezvous after situational awareness sensors reveal an unsafe condition in the vicinity of the target, the servicer will simply continue to drift below the target, merely passing it by.

Third, the Hohmann raise maneuvers are naturally fuel efficient as the Hohmann transfer is generally the optimal minimum ΔV transfer between orbits of different altitudes. However, the altitude raises can be performed by other types of transfers provided that the required ΔV remains with the mission budget. It should be noted that due to the orbital dynamics inherent at the GEO altitude, the ΔV associated with these maneuvers are small, and it may be advantageous to design-in additional out-of-plane maneuvers for the purpose of improving observability for angles-only relative navigation.

PROXIMITY OPERATIONS AND CAPTURE

The proximity operations phase of AR&C begins with the maneuver by which the servicer departs the final co-elliptic drift segment and embarks upon a trajectory that will bring it to the proper location for

safety ellipse insertion some time later. This trajectory segment is computed using Lambert targeting and is designed to be passively safe in the sense that the servicer will not collide with the target if the safety ellipse insertion maneuver should be missed due to an onboard systems failure or a decision to abort the safety ellipse insertion. The simulated trajectory to the safety ellipse insertion location, the subsequent safety ellipse motion after insertion, and the passively safe short term drift motion were the insertion maneuver missed are all shown in Figure 3.

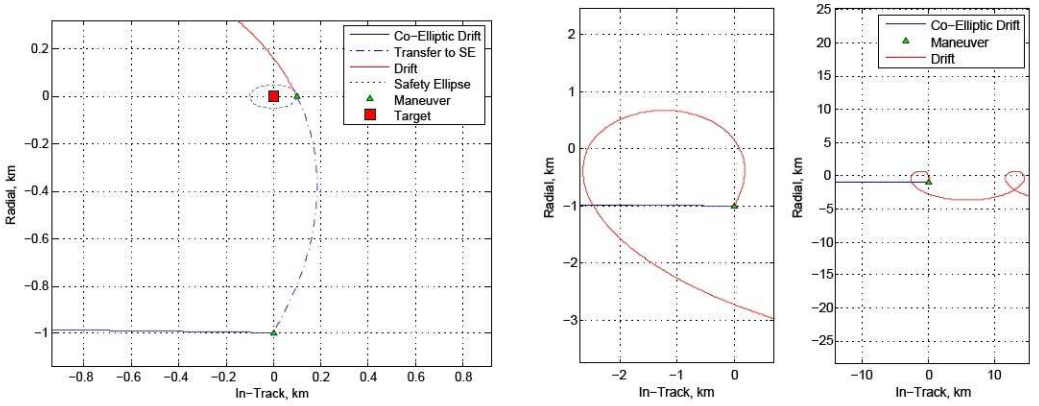

(a) Simulated Proximity Operations Trajectories

(b) Safe Natural Drift After Missed Safety Ellipse Insertion Maneuver

Figure 3. Proximity Operations Trajectories with Safe Drift

The time of flight selected for the transfer to the safety ellipse is 2 hours. From Figure 3(a) it is clear the servicer will not collide with the target if the safety ellipse insertion maneuver is not performed, though it does pass near the target. Trajectory dispersion analysis will be employed in future studies to refine the design of the transfer to the safety ellipse and ensure non-collision during drift at a sufficient confidence level. However, the long term drift motion carries the servicer well clear of the target for an extended period of time, as shown in Figure 3(b). Table 3 presents the magnitudes of the maneuvers performed to initiate the transfer to the safety ellipse and to perform the safety ellipse insertion upon arrival at the insertion location.

Table 3. Safety Ellipse Insertion Maneuver Magnitudes

Maneuver	L^1 Norm Magnitude (m/s)
Safety Ellipse Transfer Start, ΔV_5	0.222713
Safety Ellipse Insertion, ΔV_6	0.166525

Summing the maneuver magnitudes given in Table 2 and Table 3 yields a total ΔV of 1.833 m/s for the co-elliptic rendezvous and safety ellipse insertion. This is the result of our choices for the desired co-elliptic drift segment times, the initial altitude difference and the schedule of altitude changes, the use of Hohmann transfers for the altitude raises, the selected time of flight for the transfer to the safety ellipse insertion coordinates, and the chosen initial epoch, which determines the insertion location along the safety ellipse. Varying any of these parameters will yield a rendezvous and proximity operations trajectory set with a different total ΔV.

Safety Ellipse Design

Safety ellipses can be constructed in a variety of ways, including eccentricity vector and orbit plane control.[1] A small difference between the orbit planes and eccentricities of the servicer and target orbits will produce periodic Radial and Cross-Track differences in position that are never simultaneously zero by virtue

of judicious initial phasing. The motion is made repetitious with no In-Track drift by exactly matching the semimajor axes (periods) of the servicer and target orbits while taking into account the eccentricity of the target's orbit.[2] The equations of motion for safety ellipses can be derived in Hill's frame using Hill's Equations and phase space considerations[3] or geometry and kinematics.[4]

The result is an out of plane elliptical relative motion trajectory of the servicer with respect to the target spacecraft that never crosses the target's velocity vector. This provides a degree of passive safety in terms of collision avoidance. Small thruster pulses can be used to maintain the safety ellipse motion in the presence of natural orbit perturbations. A convenient parametrization[3] of the safety ellipse design variables in Hill's frame is depicted in Figure 4.

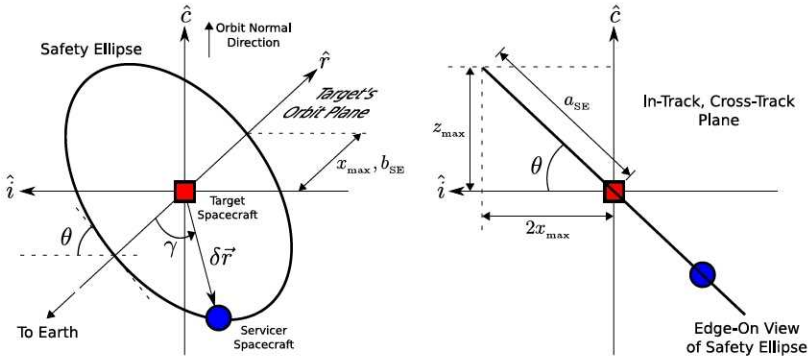

Figure 4. Safety Ellipse Geometry

The $x_{\max}$ parameter is the maximum radial extent of the safety ellipse motion and is the closest that the servicer's center of mass will be to the target's center of mass during safety ellipse motion that is centered on the target spacecraft with no In-Track drift. $z_{\max}$ is the maximum Cross-Track extent and together these parameters constrain the size and orientation of the safety ellipse. The orientation of the safety ellipse is parametrized by θ, the angle by which the plane of the safety ellipse motion is tilted about the Radial axis relative to the target's orbit plane. The size of the safety ellipse can be parametrized by its semiminor and semimajor axes, denoted by b_{SE} and a_{SE}, respectively.

Additionally, the center of the safety ellipse can be offset from the target's center of mass along the In-Track direction by an amount y_{c} and an In-Track drift or "walk" rate, denoted by $\dot{y}_{\mathrm{c}}$, can be specified for the safety ellipse motion. A "walking safety ellipse" is produced when $\dot{y}_{\mathrm{c}} \neq 0$, yielding a relative motion that spirals around the In-Track axis towards or away from the target depending on the signs of the initial In-Track coordinate and $\dot{y}_{\mathrm{c}}$. Walking safety ellipses are not exactly centered on the In-Track axis because they have a radial bias proportional to $\dot{y}_{\mathrm{c}}$.

Finally, the initial location along the safety ellipse (at the time of safety ellipse insertion) is denoted by γ_0, the initial value of the safety ellipse polar angle γ that parametrizes the location of the servicer along the safety ellipse at any given time. γ_0 can be chosen judiciously to ensure natural maintenance of a favorable angle between the sun, the servicer, and the target throughout the safety ellipse motion.[3] Figure 5(a) depicts this angle, denoted by ζ, in the context of the target's visibility to the servicer due to solar illumination. This visibility model assumes a spherical target body and simple illumination modeling, which provides a reasonably accurate visibility constraint for this study; a more realistic visibility calculation would account for the target spacecraft geometry, surface reflectivity properties, and so on.

Keeping ζ small serves two important purposes. First, it ensures that the target will not shadow the servicer's solar arrays. Second, it ensures target visibility to the servicer by virtue of a sufficient portion of the target being illuminated by sunlight and by preventing the servicer from having to point its sensors in the general direction of the sun when viewing the target. γ_0 is computed to achieve these conditions as follows:

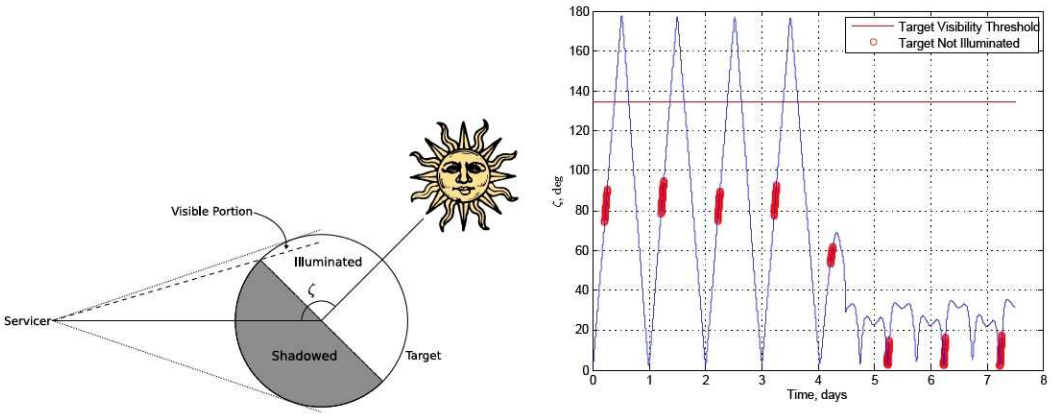

(a) Target Spacecraft Visibility Geometry

(b) Sun Angle Throughout Rendezvous and Proximity Operations

Figure 5. Target Visibility as a Function of Solar Illumination

$$\hat{r}_{SUN/TARG} = \left(\vec{r}_{SUN} - \vec{r}_{TARG}\right) / \left(\|\vec{r}_{SUN} - \vec{r}_{TARG}\|\right) \tag{2a}$$

$$[\bar{\rho}_i]_{ECI} = \hat{h} \times \left(\hat{r}_{SUN/TARG} \times \hat{h}\right) \tag{2b}$$

$$[\bar{\rho}_i]_{RIC} = T_{RIC}^{ECI} [\bar{\rho}_i]_{ECI} \tag{2c}$$

$$\gamma_0 = \arctan\left(\frac{-[\bar{\rho}_i]_{RIC_{\hat{i}}}}{[\bar{\rho}_i]_{RIC_{\hat{r}}}}\right) \tag{2d}$$

where $\vec{r}_{SUN}$ is the ECI position vector of the Sun, $\vec{r}_{TARG}$ is the ECI position vector of the target spacecraft, $\hat{h}$ is the unit vector normal to the target's orbit plane, and T_{RIC}^{ECI} is the matrix that transforms from the ECI frame to the target's RIC frame. All of these quantities are computed at the time at which the servicer is to be inserting onto the safety ellipse. $\vec{r}_{SUN}$ was computed as a function of time using an accurate approximation algorithm (Reference 5, pp.263-7).

The initial epoch for the rendezvous simulation and all time of flight parameters were presented previously, leading to the epoch of safety ellipse insertion that determines γ_0. The safety ellipse design parameters were selected to produce a static (non-walking) safety ellipse centered on the target spacecraft that projects a 50×50 meter circle in the Radial, Cross-Track plane. This keeps the servicer close enough to the target to perform accurate pose estimation and acquire detailed situational awareness imagery. The resulting set of safety ellipse design parameters is given in Table 4 and produces a safety ellipse with a semimajor axis of approximately 111.8 m and a semiminor axis of 50 m, with the plane of the safety ellipse motion inclined to the target's orbit plane by approximately $26.57°$. Thus the distance between the servicer and target spacecraft will vary between 50 and 111.8 meters throughout the safety ellipse motion.

Figure 6 shows the simulated safety ellipse motion subsequent to insertion for approximately 3 days (3 periods of the target's orbit at approximately GEO altitude). ζ remains less than $35°$ while the servicer is on the safety ellipse, as shown in Figure 5(b) for the period of time beginning at approximately 4.5 days. Note that the minimum achievable value of ζ in any scenario depends on the solar beta angle, which is a function of the epoch. Note also that the time required for the servicer to complete one revolution on the safety ellipse is equal to one of the target's orbit periods. For this reason the servicer will spend at least one day on the safety ellipse to circumnavigate the target and acquire the necessary sensor data.

Figure 5(b) shows the time history of the visibility of the target to the servicer. The ζ angle threshold for

Table 4. Safety Ellipse Design Parameters

Parameter	Value
Maximum Radial Extent, $x_{\max}$, m	50
Maximum Cross-Track Extent, $z_{\max}$, m	50
In-Track Offset, y_c, m	0
Walk Rate, $\dot{y}_c$, m/s	0
Initial Location on SE, γ_0	270.411544°

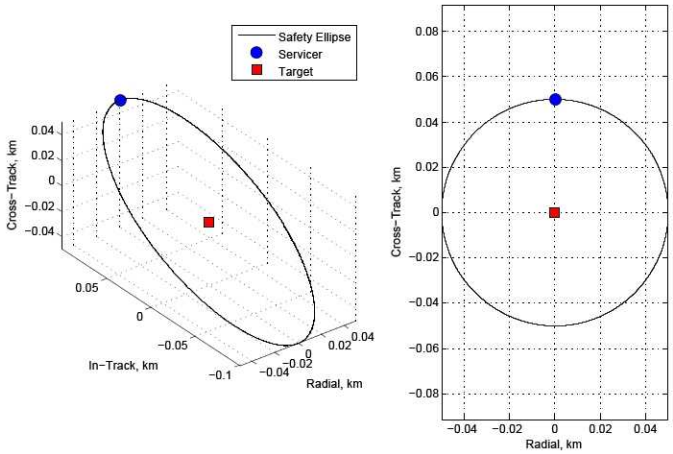

Figure 6. Safety Ellipse Motion Simulated For Three Days

visibility $(135°)$ is clearly marked, and periods during the which the target spacecraft happens to not have any sunlight shining on it are marked as well. An algorithm found on p.294 of Reference 5 was used to determine when the sun is shining on the target spacecraft. Together, these constraints define the intervals during which bearing angle measurements are available during the rendezvous.

Capture

The servicer will spend a sufficient amount of time (perhaps one or several target orbit periods) on the safety ellipse to characterize the target, gather situational awareness data, and acquire stable and accurate estimates of the target's relative position, attitude, and the rates thereof. Relative navigation will be primarily performed by pose estimation sensors and algorithms.

Once the situation is deemed safe and relative navigation is stable, the servicer will depart the safety ellipse, flying a short trajectory that will intercept the target spacecraft's capture axis. The capture axis is a fixed direction defined in the target's body frame along which the servicer will perform a gentle approach until close enough to use its robotic arms to grapple and capture the target.

Kinematics and dynamics are applied in straightforward fashion to transform the desired position over time of the servicer in the target's body frame along the capture axis into position over time in the target's RIC frame. This allows the servicer to use Lambert or CW targeting to compute the maneuvers necessary to fly along the capture axis as the target's inertial attitude evolves. Other considerations include the appropriate placement and actuation of the servicer's thrusters so as to keep target plume impingement within acceptable levels during proximity operations and capture, though such issues are beyond the scope of this paper.

The servicer's motion along the capture axis nominally consists of a series of holds and constant rate approaches; retreats will occur only when necessary, e.g., for an abort or the repeat of a grapple attempt.

A key factor during the capture axis approach phase is the attitude state of the target. In this study we are examining the case of a non-cooperative target spacecraft that cannot control its attitude and will therefore be in whatever attitude state is produced by the natural evolution of its attitude under various perturbations subsequent to attitude control system failure. The control authority offered by the servicer's thrusters and the limits of its fuel supply will restrict the target spacecraft spin states that can be coped with. We assume that the target spacecraft will only offer a limited number of hard points at which it can be grappled, and the servicer's robotic arms will be of limited length; these factors constrain the available capture axis directions in the target's body frame.

The amount of ΔV required of the servicer for the capture axis approach is proportional to r, ω^2, and $\sin(\theta)$, where r is the distance between the servicer and the target along the capture axis, ω is the magnitude of the target's angular velocity vector, and θ is the angle between the capture axis and the target's angular velocity vector. The worst case for θ is $\pi/2$, which occurs when the capture axis and angular velocity vector are orthogonal. The impact of θ decreases as it tends to 0 or π; at those extremes the spin state of the target no longer affects the required capture ΔV, and this is intuitively satisfying. For the cases when θ is not 0 or π, ΔV increases linearly with r and quadratically with ω. Thus, the faster the target is spinning and/or the farther away the servicer is, the larger the total capture ΔV. The impact of r means that performing a hold on the capture axis can be costly in terms of ΔV; the cost increases with ω, θ, the value of r at which the hold is performed, and the amount of time spent holding.

Obviously the rotation rate of the target vehicle is a key GN&C driver during the capture phase. For this paper we assume a target vehicle with a weathercock shape for which uncontrolled motion eventually settles the vehicle into a sun pointing attitude. Our analysis (not presented here) shows maximum rates on the order of 0.0075 RPM ($0.045^\circ/s$). The relatively small attitude rates predicted for this Nominal Case require very small total capture ΔV and so we include two additional cases with larger attitude rates in order to explore the capture ΔV requirements for more problematic attitude states that other non-cooperative target spacecraft might present. In Case 1, the target spins at 0.04167 RPM (0.25°/s) and in Case 2 the target spins at 0.16667 RPM (1.0°/s).

Figure 7 shows the sequence of events and associated trajectories for the capture. The servicer first departs the safety ellipse and flies a short trajectory to acquire the capture axis. The servicer then begins flying along the capture axis according to the schedule presented in Table 5, bringing it to within 1 meter of the grapple point on the target. The servicer then holds there while its robotic arms move in, grasp the target, and rigidize the spacecraft stack. The distance of the grapple point from the target's center of mass along the capture axis is 5 meters. The servicer's attitude throughout is such that it points its relative navigation and situational awareness sensors towards the target at all times. The servicer will then match the target's attitude during the end of the capture axis approach in preparation for grapple and capture.

Table 5. Capture Axis Approach Profile

Phase	Time (minutes)	Approach Rate (cm/s)
Hold at 30 meters	20.0	0.0
Approach to 10 meters	6.67	5.0
Hold at 10 meters	10.0	0.0
Approach to 1 meter	3.0	5.0
Hold at 1 meter	10.0	0.0

The point along the safety ellipse at which the servicer departs and the time of flight (2 hours) to reach the starting point on the capture axis were selected to provide reasonable maneuver magnitudes and to yield drift motion that is passively safe if the servicer loses the ability to maneuver prior to capture axis acquisition or otherwise decides to abort the capture axis approach. Figure 7 shows the drift of the servicer for 6 hours, and it is clear that the drift motion naturally takes the servicer well clear of the target. This drift motion was also propagated for several days and took the servicer ever further from the target, looping along the In-Track axis.

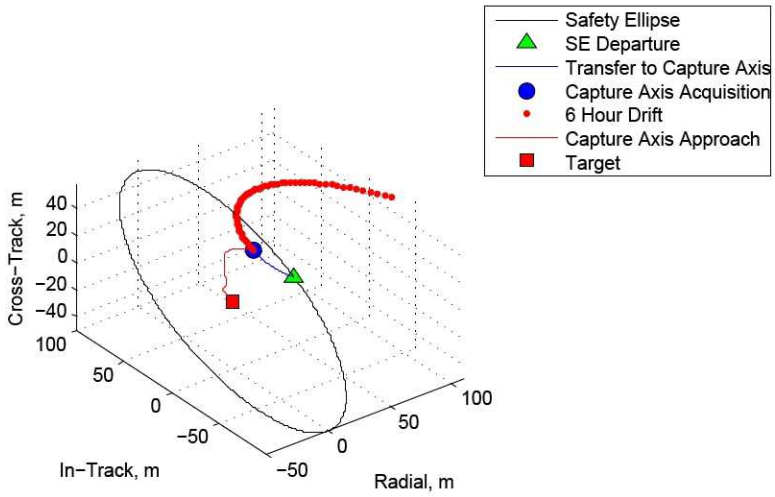

Figure 7. Transition to Capture Axis Approach from Safety Ellipse

Figure 8 shows the capture axis approach distance versus time, corresponding to the schedule given in Table 5, along with a close-in view of the capture axis approach trajectory. Table 6 gives the maneuver magnitudes for the capture sequence, beginning with safety ellipse departure, for the Nominal attitude case and the other two higher attitude rate cases. The amounts of ΔV required for the $0.045°/s$ and $0.25°/s$ cases are relatively small, but the $1.0°/s$ case results in a significantly larger ΔV requirement. The angle θ between the capture axis and the target's angular velocity vector for all three cases was approximately $84°$, representing an essentially worst case scenario in terms of θ.

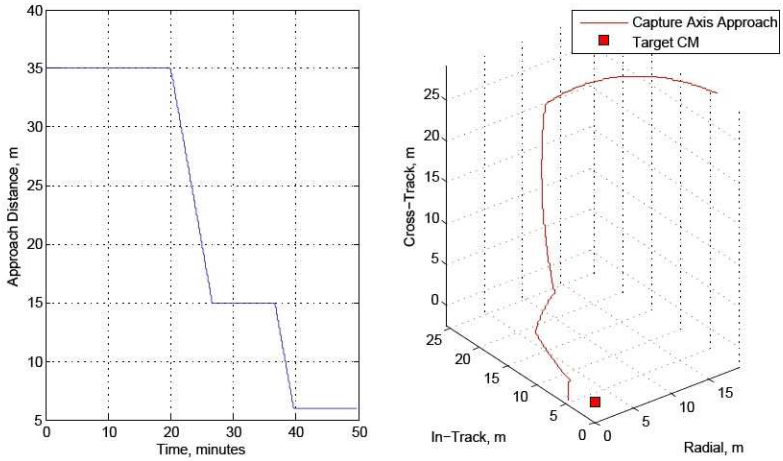

Figure 8. Approach Distance vs. Time and Capture Axis Approach Trajectory in the RIC Frame

Overall AR&C ΔV Budget

Summing the ΔV values in Tables 2, 3, and 6 yields total AR&C ΔV values of 2.286, 3.942, and 23.839 m/s for the Nominal, Case 1, and Case 2 target attitude rate cases, respectively. Since the Nominal tumble is considered to be fairly representative of the likely tumble state for a failed spacecraft at GEO, we assume that Case 1 ($0.25°/s$) serves well to bound the worst case target attitude as it is tumbling approximately 5.5 times

Table 6. Capture Maneuver L^1 Norm Magnitudes

Maneuver	Nominal Case ($0.045°/s$)	Case 1 ($0.25°/s$)	Case 2 ($1.0°/s$)
Safety Ellipse Departure (m/s)	0.019	0.019	0.019
Capture Axis Acquisition (m/s)	0.037	0.184	0.720
Capture Axis Approach (m/s)	0.397	1.906	21.267
Totals (m/s)	**0.453**	**2.109**	**22.006**

faster than the nominal case. Nevertheless, Case 2 serves to illustrate that the capture ΔV requirements can quickly become significant even for modest tumble rates such as $1.0°/s$.

Using the Case 1 tumble rate to size the general AR&C ΔV budget for this sort of mission would yield a total ΔV of 4 m/s, but there are other factors not yet considered. These include, but are not limited to, impacts to the total ΔV budget from maneuver execution errors, impulsive versus finite burn maneuver modeling, absolute and relative navigation errors, thruster pointing limitations, general mid-course correction maneuvers, changes to the overall AR&C sequence due to anomalous events (e.g., aborts, collision avoidance maneuvers, or retreats and re-approaches along the capture axis), and safety ellipse maintenance maneuvers. Since thorough analysis of all these factors has yet to be performed, we have made the preliminary estimate that the total ΔV required for AR&C could be larger than the ideal case by a factor of 5, yielding a total AR&C ΔV of 20 m/s.

Thus, for the purposes of sizing a servicing mission campaign in which the servicer will visit multiple (potentially dissimilar) targets in series, we are assuming that a total ΔV of 20 m/s will cover the entire AR&C phase for each target. Further studies will serve to more accurately bound the amount of AR&C ΔV capability generally required of the servicer.

RELATIVE NAVIGATION

A preliminary analysis was conducted to examine the feasibility of the relative navigation concept for the GEO rendezvous and capture scenario, given specific assumptions regarding measurement type and availability, and navigation estimation methodology. Table 7 presents the absolute Earth-Centered Inertial (ECI) initial state vectors for the servicer and target spacecraft at the chosen initial epoch for the rendezvous simulation of Julian Date (JD) 2456924.5 (September 24$^{\text{th}}$, 2014, 00:00:0.000 UTC). These initial conditions place the servicer at the desired starting point for the co-elliptic portion of the AR&C phase as shown in Figure 2, approximately 30 km below and 300 km behind the target.

Table 7. Servicer and Target Spacecraft Earth-Centered Inertial Initial Conditions at JD 2456924.5 for Co-Elliptic Rendezvous Start

State	Servicer	Target
$x_{_{ECI}}$, km	2494.88826130217	2795.42298831499
$y_{_{ECI}}$, km	-42102.2290061097	-42113.4361464975
$z_{_{ECI}}$, km	-155.416694694079	-164.560354309237
$\dot{x}_{_{ECI}}$, km/s	3.06711160082855	3.06465389184191
$\dot{y}_{_{ECI}}$, km/s	0.181526811236294	0.20322752662348
$\dot{z}_{_{ECI}}$, km/s	-0.09275570195593	-0.0926400276645387

Sensors

The servicer spacecraft is assumed to carry sensors capable of measuring range and bearing angle from the servicer spacecraft to the target, for performing relative navigation. A notional AR&C sensor suite was conceived to provide redundant measurements throughout the rendezvous, proximity operations, and capture

phases of the non-cooperative GEO rendezvous scenario. The AR&C sensors would include cameras (for bearing measurements and pose), a flash or scanning lidar (range, bearing, and pose), a laser range finder (range measurements), and an infrared camera. Long-range bearing measurements (outside of 5 km separation) made by cameras would be dependent on solar illumination of the target. Bearing measurements inside of 5 km would be made by a lidar, an active sensor. The laser range finder is assumed to provide range measurements out to 20 km separations. Inside 5 km, the lidar would provide a redundant source of range measurements. It should be noted that 5 km separations may be outside of the range in which existing lidar systems could reliably operate without cooperative retro-reflector targets on the target spacecraft; however there is intentional overlap between the sensing capability of cameras and laser range finder in this range.

Relative Navigation Simulation

The Orbit Determination Toolbox (ODTBX)[6] was used to propagate reference trajectories for the servicer and target spacecraft, compute required rendezvous maneuvers, generate simulated range and bearing measurements, and perform state estimation by processing the simulated measurements. Estimated states for this feasibility study included the absolute inertial states of the servicer and target spacecraft. Table 8 provides the initial state error covariances for the servicer and target.

Table 8. Servicer and Target Spacecraft Initial State Error Covariances

State	Servicer	Target
x_R, m	10	100
x_I, m	100	1000
x_C, m	10	100
$\dot{x}_R$, mm/s	0.1	1
$\dot{x}_I$, mm/s	1	10
$\dot{x}_C$, mm/s	0.1	1

The sequence of simulated maneuvers, as described in Table 1, including the entire rendezvous trajectory, safety ellipse insertion, and 3 days spent on the safety ellipse, spans just less than 8 days. Each maneuver is calculated using the estimated states of the servicer and target spacecraft prior to the maneuver, and the resulting impulsive ΔV is applied to the target and servicer reference trajectories. No closed-loop control or mid-course correction maneuvers were included in the simulation.

Simulated Measurements

Angles-only relative navigation is assumed when the servicer is $>$ 20 km from the target. Range measurements are assumed to be available, in addition to bearing, when the servicer is $\leq$ 20 km from the target. It is also assumed that the servicer will be performing pose measurements (direct measurements of position, attitude, and rates thereof relative to the target) during the proximity operations and capture phases, when the servicer is $\leq$ a few hundred meters from the target. However, only the range and bearing measurements are modeled in this study.

Bearing measurements are simulated as a line-of-sight vector in inertial space, from the servicer spacecraft to the target. While range measurements are available continuously when the servicer is $\leq$ 20 km from the target, the availability of bearing measurements is limited by solar illumination of the target when the servicer is $>$ 5 km from the target. This solar illumination constraint consists of two aspects. First, the target must be receiving sunlight (i.e., not shadowed by the Earth). Second, the phase of the target's illumination with respect to the servicer must cause a sufficient quantity of light to be reflected toward the servicer.

The periods of measurement availability are shown in Figure 5(b) based on the ζ angle constraint and solar illumination of the target. Combined with the distance constraints outlined in this section, the result is that bearing measurements are available for 79.4 hours out of the 108 hours prior to safety ellipse insertion, or

approximately 73% of the time up to safety ellipse insertion. Range measurements are available for 45.7 out of the 108 hours, approximately 42.3% of the time.

One-sigma bearing measurement errors (or errors in line-of-sight direction) were simulated as one milliradian in each component of the line-of-sight vector. Errors in measured range were simulated as the larger of 1% of the actual range, or one meter. Additionally, the servicer spacecraft is assumed to carry a GPS receiver capable of receiving weak GPS signals and producing an estimate of the inertial state of the servicer spacecraft in the sparse GPS signal environment present at GEO.[7] In application, it is assumed that the pseudorange measurements recorded by the GPS receiver on the servicer spacecraft would be processed in the navigation filter. In this simulation, inertial positions for the servicer spacecraft were processed as measurements. A one-sigma noise covariance of 10 m in each component was assumed for simulated servicer position measurements.

Relative Navigation Results

Figure 9(a) and Figure 9(b) show relative position errors plotted in the RIC frame from a representative single simulation run, at two difference scales. Figure 10(a) and Figure 10(b) show the corresponding relative velocity errors. Safety ellipse injection position error, which includes the effect of navigation errors on the maneuver execution accuracy, was approximately 5.1 m for this case.

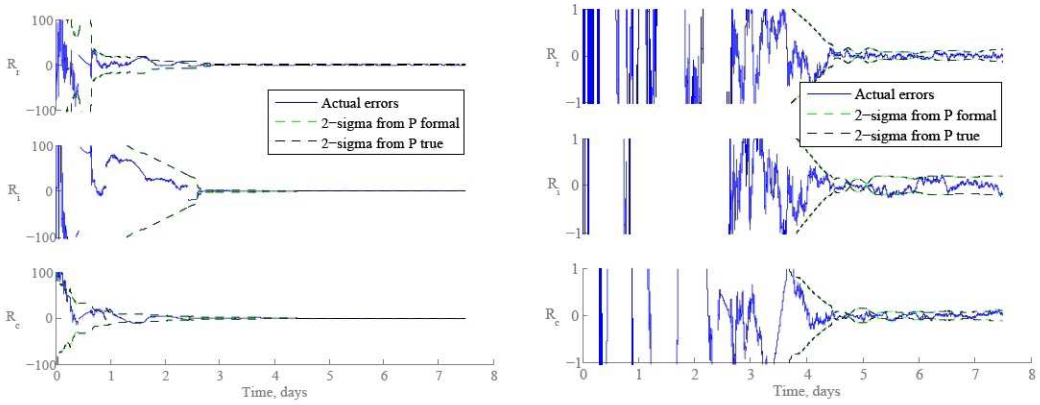

(a) Relative Position Errors, m

(b) Relative Velocity Errors (Zoom), m

Figure 9. Relative Position Errors

Table 9 provides relative position and velocity error statistics from the end of each trajectory segment, compiled from approximately 80 simulation cases. Both position and velocity errors are reduced significantly during the second co-elliptic drift segment, corresponding to the period between approximately 1 and 2.5 elapsed days. Velocity errors are reduced early in the second co-elliptic segment, while position errors take longer to come down. Range measurements become available towards the end of the second co-elliptic segment, when the distance between the servicer and target becomes less than 20 km. Safety ellipse injection errors for these cases, which include the resulting effects of the navigation error on the maneuver execution performance, varied between 0.3 and 68 meters, with a mean of 20 meters.

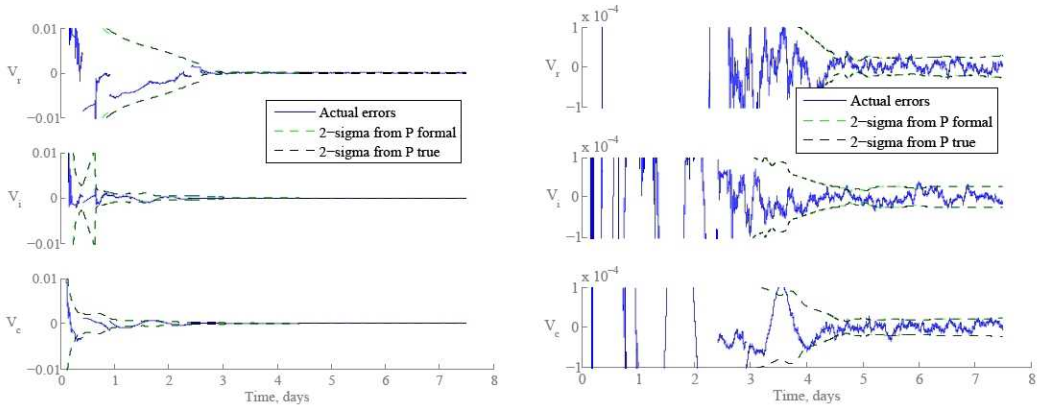

(a) Relative Velocity Errors, m/s

(b) Relative Velocity Errors (Zoom), m

Figure 10. Relative Velocity Errors

Table 9. Relative Position and Velocity Error Statistics

	Relative Position, m				Relative Velocity, mm/s			
Segment	Min.	RMS	Max.	σ	Min.	RMS	Max.	σ
1st Co-Elliptic drift	17.349	99.032	314.108	50.171	0.590	7.553	25.192	3.987
1st Hohmann raise	9.094	59.718	138.517	30.643	0.584	4.128	9.428	2.236
2nd Co-Elliptic drift	1.031	15.990	39.498	9.106	0.165	1.134	2.731	0.647
2nd Hohmann Raise	0.186	1.737	3.442	0.732	0.029	0.149	0.368	0.068
3rd Co-elliptic Drift	0.016	0.185	0.422	0.078	0.007	0.026	0.062	0.010
Transfer to Safety Ellipse	0.017	0.092	0.214	0.042	0.005	0.022	0.043	0.008
Safety Ellipse Insertion	0.010	0.114	0.269	0.057	0.005	0.020	0.040	0.008

MULTI-TARGET RENDEZVOUS

If a servicer spacecraft can service multiple spacecraft before the end of its life, the value of the mission is obviously greatly increased. To achieve this the servicer must rendezvous with each target spacecraft to be serviced, and the order in which a given set of target spacecraft are rendezvoused with strongly influences the total ΔV required. Thus, choosing a ΔV-efficient order for visiting the targets allows the servicer to visit more targets for a given amount of ΔV or visit a given number of targets for less ΔV. This presupposes that other constraints (e.g., logistics or target availability) do not take precedence and dictate the order in which targets are serviced irrespective of the impact on total ΔV required.

Problem Statement and Characterization

The goal is therefore to choose the order in which a given set of target spacecraft are rendezvoused with such that the total number of targets that the servicer is able to visit is maximized. Generally this translates to minimizing the total required ΔV. This is similar in character to the famous Traveling Salesman problem, in which the order for visiting a set of cities is to be optimized to minimize the total path distance traveled. Strictly optimizing the order in which target spacecraft are visited such that the total ΔV is formally minimized is daunting since, like the Traveling Salesman problem, it is an NP-complete combinatorial optimization problem. This is because the number of permutations of target spacecraft order is practically impossible to exhaustively sample for an interesting number of target spacecraft.

Solution Methodology

The Series Method algorithm offers a computationally efficient means of obtaining a good, if perhaps suboptimal,* solution to the problem. The Series Method was originally developed for designing interplanetary science missions to tour Near-Earth Asteroids and has been used successfully on such problems.[8] In the Series Method, the order for visiting target spacecraft is constructed in series, choosing each subsequent target after the first on the basis of minimum ΔV to reach the next target, akin to a computer chess program that only looks one move ahead when selecting its next move. Details about the development, structure, and characteristics of the Series Method algorithm can be found in Reference 8. If a particular target spacecraft must be visited first, this can be specified; elsewise the algorithm will choose the first target by trying each target as the first when constructing the itineraries and then selecting the choice of first target that serves to maximize the total number of target visits achieved.

To see the computational advantage of the Series Method compared to an exhaustive search, we examine the total number of ΔV calculations required. In an exhaustive search all the permutations of target order must be treated and the ΔV to travel between targets must be computed for each permutation. The resulting number of ΔV calculations for the exhaustive permutation search, N_p, is therefore given by

$$N_p = (S-1)\frac{T!}{(T-S)!} \tag{3}$$

where S is the number of target spacecraft to visit and T is the total number of available target spacecraft to choose from. Herein we shall consider cases where $S = T$, in which case Eq. 3 reduces to $N_p = (T-1)\,T!$.

The number of ΔV calculations performed in the Series Method, N_s, assuming that each target is tried as the first target in order to find the choice of first target that maximizes the number of targets that can be visited, is

$$N_s = T\sum_{k=1}^{S-1} T - k \tag{4}$$

*The optimality of the Series Method has yet to be characterized and may be addressed in future studies. Subjective assessment of the character of the solutions generated by the Series Method indicates that it is likely at least near-optimal

A comparison of N_p and N_s is provided in Table 10 for a range of T values (target spacecraft population sizes), assuming that $S = T$. The Series Method is clearly far less computationally expensive than the exhaustive search, allowing target spacecraft populations of interesting sizes (e.g., $T > 20$) to be handled readily on standard workstation computers. By contrast, treating such population sizes with an exhaustive search would require large supercomputers. However, the number of calculations required for exhaustive search solutions for small target populations ($T < 7$) are tractable, enabling future studies that will characterize the optimality of the Series Method statistically.

Table 10. Number of ΔV Calculations Required by Exhaustive Search and Series Method

T	N_p	N_s
3	12	9
4	72	24
5	480	50
7	30240	147
10	3.26592×10^7	450
20	4.622514×10^{19}	3800
30	7.692333×10^{33}	13050
40	3.182070×10^{49}	31200
100	9.239295×10^{159}	495000

Other numerical methods for solving this orbital version of the Traveling Salesman problem might also be pursued, such as Simulated Annealing and/or Genetic Algorithms. Such algorithms are known to be capable of providing practical optimal or near-optimal solutions to Traveling Salesman type problems and may be explored in future work. Their efficacy and computational expense would be compared to the Series Method, as they might offer only slightly improved performance but with increased complexity, additional computational expense, and decreased robustness.

Rendezvous Sequence

The rendezvous sequence between any two targets consists of making the servicer's orbit co-elliptic with the target, as shown in Figure 1, and then allowing the relative orbital drift to bring the servicer to the point of AR&C start. Rendezvous, proximity operations, and capture operations then proceed as described previously. Finally, the target spacecraft is serviced and the servicer then either proceeds to the next target or disposes of itself if it does not have enough fuel remaining to continue servicing.

The total ΔV required for AR&C is assumed to be 20 m/s for each target, as specified previously. All that remains is to compute the total ΔV required to make the servicer's orbit co-elliptic with the target's orbit, and a computationally efficient means of doing this has been devised. The full derivation of these co-elliptic rendezvous maneuver equations is omitted here for brevity, but a brief description follows.

Co-Elliptic Rendezvous Maneuvering

The co-elliptic rendezvous maneuver equations were inspired by a scheme developed for impulsive mean orbital element control[9] and consist of matching the orbit plane (i and Ω) of the target, matching the line of apsides (ω), and matching the eccentricity and semimajor axis (e and a). If the servicer begins from a higher orbit than the target, plane matching is performed first to reduce the required ΔV. Also, line of apsides matching is clearly unnecessary if the target's orbit is perfectly circular. A new development is that the equations for the plane matching maneuvers were derived from the form of Gauss' equations that utilize the equinoctial (nonsingular) elements in lieu of the classical Keplerian elements.[10] The use of Gauss' equations in equinoctial elements for deriving the complete set of orbital maneuvering equations will be examined in future work.

Satellite Re-Fueling Analysis

While super-synching non-functional satellites has been the focus of this study thus far, the concept of re-fueling satellites in GEO is now examined to demonstrate the utility of the Series Method for designing multi-target rendezvous missions. Providing extra fuel to otherwise healthy satellites that would require replacement due to the exhaustion of their fuel would allow satellite operators to gain continued usage of their existing satellites for the nominal cost of a re-fueling service rather than the much higher cost of fabricating and launching replacement satellites.

In addition to analyzing the capabilities of a single servicer spacecraft to re-fuel a population of target satellites, the concept of pairing the servicer with a fuel depot is also considered. The goal is to ascertain whether using an on-orbit fuel depot enhances the overall capability of the re-fueling architecture. For the with-depot case it is assumed that the servicer and the depot are deployed on a single launch vehicle (Delta-IV Heavy); it is also assumed in the without-depot case that the same launch vehicle is used to deploy the servicer alone.

Two target satellite populations are examined in this study. The first population is designated Group 1 and consists of 39 US GEO satellites that use Hydrazine fuel. The second population is designated Group 2 and consists of 47 various GEO satellites with relatively disparate orbit planes (as compared to Group 1).

A study was performed in the NASA GSFC Mission Design Lab (MDL) to produce realistic designs for the servicer spacecraft and the fuel depot. While those designs were complete and covered all spacecraft subsystems, only the spacecraft design parameters necessary for this re-fueling architecture study are presented herein. The servicer spacecraft's thruster has a specific impulse of 210 seconds and the fuel mass parameters of the spacecraft designs are summarized in Table 11.

Table 11. Spacecraft Fuel and Dry Masses for Re-Fueling Architecture Study

	With-Depot	Without-Depot
Servicer Dry Mass (kg)	2014	2300
Servicer Fuel Mass (kg)	560	3989
Fuel Depot Dry Mass (kg)	1500	N/A
Fuel Depot Fuel Mass (kg)	2215	N/A

An algorithm was developed to control the servicer's behavior during re-fueling. First, the Series Method is used to select the next target spacecraft. Before proceeding to the next target, the servicer evaluates its situation using a logical decision-making tree; as long as the servicer has enough fuel to re-fuel the next target *and* return to the fuel depot afterward, it will continue to re-fuel targets, one after the other. The servicer also monitors its fuel supply to ensure that it always has enough fuel remaining to return to the depot and boost itself and the depot to a disposal orbit, regardless of whether the depot still contains fuel.

As soon as the servicer has only enough fuel remaining for disposal, accounting for the depot's remaining fuel supply, the servicer will perform the disposal and end the mission. Additional analysis has indicated that the depot's orbit plane will drift by approximately 0.5° between visits by the servicer, so the servicer corrects the depot's orbit plane at each visit. Also, the depot's orbit plane will be the same as that of the first target serviced, but its altitude is 100 km higher. The altitude for disposal is 300 km above GEO.

To rendezvous with each target in series, the servicer spacecraft performs the necessary maneuvers to make its orbit co-elliptic with the next target spacecraft but with an altitude 127 km higher so that it can naturally drift to close distance with the target; AR&C operations begin at a distance of 300 km as described previously.

The goal of the re-fueling system is to maximize profit and usefulness, which generally translates to maximizing the number of target satellites that can be re-fueled. However, there are other ways to meter re-fueling performance and efficiency. One possible metric is the fuel delivery ratio, which is the percentage of the total fuel launched that is delivered to target satellites. Another is the mass delivery ratio, which is the percentage of the total launch mass that is delivered as fuel to the target satellites. Yet another metric might simply be

the total mass of fuel delivered, since the monetary profit of the re-fueling enterprise may be per unit mass of fuel delivered.

A series of simulations were performed to test the performances of several re-fueling scenarios. A servicer attempted to re-fuel as many of the Group 1 and Group 2 target satellites as possible, with and without a fuel depot. In the first round of simulations, 20 kg of fuel was delivered to each target satellite. The results for that round of simulations are presented in Table 12. In the second round of simulations, 100 kg of fuel was delivered to each target satellite, and these results are presented in Table 13. Data plots of the simulation results are presented in Figures 11 and 12 for the Group 1 with and without depot cases, respectively, with 20 kg of fuel being delivered to each target. Data plots for the Group 2 and 100 kg fuel delivery cases are omitted for brevity as their characters are quite similar to the plots in Figures 11 and 12.

Table 12. Re-Fueling Performance with 20 kg of Fuel Delivered to each Target Spacecraft

Case	# Sats Re-Fueled	Unused Servicer Fuel (kg)	Unused Depot Fuel (kg)	# Depot Visits	Total ΔV (m/s)	Total Fuel Delivered (kg)	Fuel Delivery Ratio	Mass Delivery Ratio
Group 1 With-Depot	26	106	0	4	1697	520	19.48%	8.27%
Group 1 Without-Depot	29	284	N/A	N/A	1561	580	15.65%	9.22%
Group 2 With-Depot	11	35	0	5	2005	220	8.03%	3.50%
Group 2 Without-Depot	16	106	N/A	N/A	1823	320	8.24%	5.09%

Table 13. Re-Fueling Performance with 100 kg of Fuel Delivered to each Target Spacecraft

Case	# Sats Re-Fueled	Unused Servicer Fuel (kg)	Unused Depot Fuel (kg)	# Depot Visits	Total ΔV (m/s)	Total Fuel Delivered (kg)	Fuel Delivery Ratio	Mass Delivery Ratio
Group 1 With-Depot	17	5	0	5	762	1700	61.37%	27.03%
Group 1 Without-Depot	21	19	N/A	N/A	928	2100	52.90%	33.39%
Group 2 With-Depot	9	9	0	5	1425	900	32.54%	14.31%
Group 2 Without-Depot	14	57	N/A	N/A	1300	1400	35.61%	22.26%

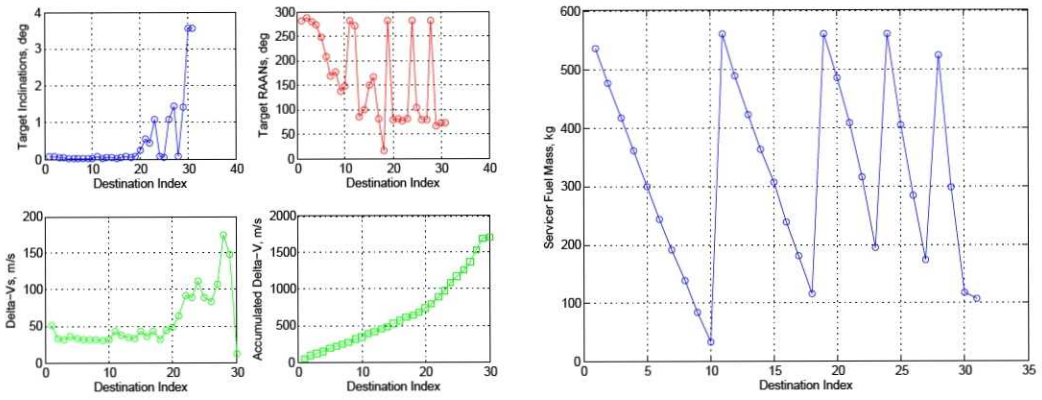

(a) Target Inclinations, RAANs, and ΔV Requirements

(b) Servicer Fuel Mass Evolution

Figure 11. Simulated Re-Fueling Performance With Depot for Group 1

The general trend is that the servicer without a fuel depot performs better in terms of the number of target satellites that can be re-fueled, the total fuel mass delivered, and the mass delivery ratio. However, the servicer with a fuel depot tends to perform better in terms of fuel delivery ratio for the Group 1 target satellites. This is because the servicer has a lower dry mass and smaller fuel tank in the with-depot cases, meaning that it

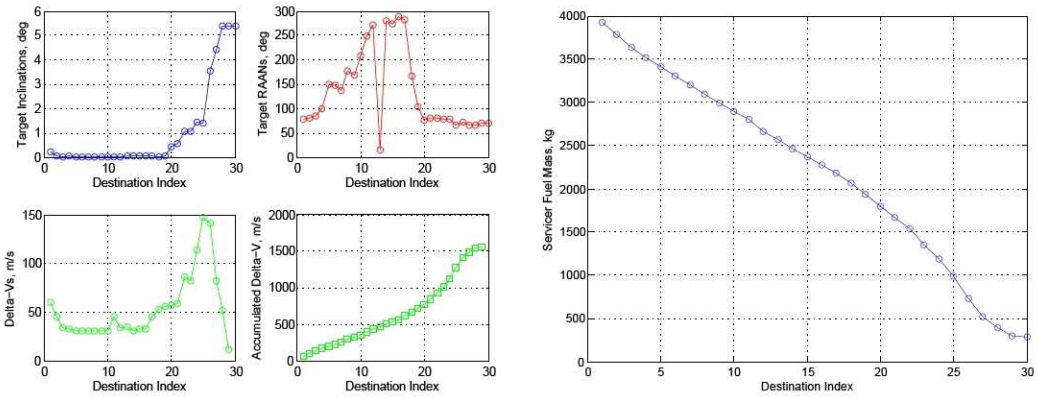

(a) Target Inclinations, RAANs, and ΔV Requirements

(b) Servicer Fuel Mass Evolution

Figure 12. Simulated Re-Fueling Performance Without Depot for Group 1

doesn't have to spend as much propellant to perform its maneuvers, as compared to the without-depot case in which the servicer is much more massive initially. However, the trips to and from the depot consume fuel that is not required in the without-depot cases. Also, the inclusion of the fuel depot's dry mass means that less of the total launch mass is fuel. This is why the with-depot cases suffer in terms of total fuel mass delivered and mass delivery ratio.

However, the with-depot re-fueling architecture may ultimately prove more efficient and achieve higher profitability if multiple launches are performed. The first launch could deploy the servicer and depot, as shown here, followed by the launches of additional fuel depots on smaller (less expensive) launch vehicles. The fuel depot is much simpler in its design than the servicer and so would be less expensive to fabricate and launch. Additional trade studies are required to properly explore this, but it could be that launching one servicer with several fuel depots performs better economically in the long run than simply launching multiple fully loaded servicers.

CONCLUSIONS AND FUTURE WORK

The costs and benefits of various spacecraft servicing architectures, and mission concepts stemming from the associated technology developments, are currently being studied at the NASA Goddard Space Flight Center. Spacecraft servicing has the potential to extend the useful lifetimes of extant spacecraft assets, reduce operational costs, and aid in the remediation of orbital debris. A servicing spacecraft could perform disposal of dead spacecraft, either by de-orbiting or boosting to a graveyard orbit. Spacecraft could be re-fueled, repaired, refurbished, or re-positioned to extend the useful life of on-orbit assets. Moreover, multiple spacecraft could be serviced by a single servicer spacecraft, greatly reducing manufacture and launch costs associated with spacecraft servicing and yielding a strong profit margin for servicing activities.

A rendezvous, proximity operations, and capture strategy was presented for a notional servicing mission to a non-cooperative spacecraft in a GEO orbit. Consideration was given to relative navigation sensor observability, navigation state observability, and safety in the design of the AR&C approach.

The Orbit Determination Toolbox was used to conduct a preliminary relative navigation analysis of the AR&C scenario. This analysis indicates that the co-elliptic rendezvous strategy is a feasible approach in terms of relative navigation uncertainty; however, a significant amount of forward work has been identified. First, the orbital dynamics in the GEO environment are slowly-changing, so it is possible to assume rectilinear motion during some phases of AR&C without incurring significant propellant costs. Furthermore, consideration could be given to inserting out-of-plane maneuvers at points during the rendezvous to improve navigation observability. Future versions of the simulation will also incorporate a realistic simulation of GPS

measurements available to a GEO spacecraft in place of processing servicer spacecraft states as a measurement. The study presented herein focused exclusively on the translational motion of the servicer while future analysis will include investigation of alternatives for estimating relative attitude in the navigation filter.

Additionally, a solution to the multi-satellite servicing problem was presented, to provide a means to select an optimal sequence of target spacecraft for a servicer performing multiple missions. This analysis is also relevant to a mission scenario that includes a fuel depot for replenishing the propellant of the servicer spacecraft. In future work, the optimality of the Series Method for solving the orbital Traveling Salesman problem will be characterized statistically.

Other forward work on a high-fidelity, closed-loop, six degrees of freedom simulation for the servicer spacecraft will also include a realistic thruster selection algorithm that will allow detailed analysis of the servicer's ability to perform proximity operations and capture without thruster plume impingement on the target spacecraft. This will permit proper sizing and orientation of the servicer's thruster ensemble. Finally, low-thrust systems such as Solar Electric Propulsion will also be considered for use on the servicer spacecraft. While low-thrust systems are far more fuel efficient than conventional thrusters, they necessitate longer transfer times, provide much less instantaneous control authority, often have a higher dry mass than conventional thrusters, and draw additional electrical power. However, the ultra-high specific impulse of low-thrust propulsion systems may still ultimately increase the number of target spacecraft that can be handled by a single servicer. Additional analysis and trade studies will shed light on the potential benefits and feasibility of using low-thrust propulsion on the servicer.

REFERENCES

[1] E. Gill, O. Montenbruck, S. D'Amico, and S. Persson, "Autonomous Satellite Formation Flying for the PRISMA Technology Demonstration Mission," 16th AAS/AIAA Space Flight Mechanics Conference, January 2006. Tampa, Florida.

[2] G. Inalhan, M. Tillerson, and J. How, "Relative Dynamics and Control of Spacecraft Formations in Eccentric Orbits," *Journal of Guidance, Control, and Dynamics*, Vol. 25, Jan-Feb 2002, pp. 48–59.

[3] B. J. Naasz, "Safety Ellipse Motion With Coarse Sun Angle Optimization," NASA-GSFC Flight Mechanics Symposium, October 2005. Greenbelt, Maryland.

[4] D. E. Gaylor and B. W. Barbee, "Algorithms for Safe Spacecraft Proximity Operations," AAS/AIAA Spaceflight Mechanics Meeting, January 2007. Sedona, Arizona.

[5] D. A. Vallado, *Fundamentals of Astrodynamics and Applications*. Microcosm Press and Kluwer Academic Publishers, second ed., 2001.

[6] Goddard Space Flight Center, "Orbit Determination Toolbox (ODTBX)," `http://opensource.gsfc.nasa.gov/projects/ODTBX/index.php`.

[7] B. Bamford, B. Naasz, and M. Moreau, "Navigation Performance in High Earth Orbits Using Navigator GPS Receiver," 29th Annual AAS Guidance and Control Conference, Feb 4-8 2006. Breckenridge, CO.

[8] B. W. Barbee, G. W. Davis, and S. Hur-Diaz, "Spacecraft Trajectory Design for Tours of Multiple Small Bodies," AAS/AIAA Astrodynamics Specialist Conference, August 2009. Pittsburgh, Pennsylvania.

[9] H. Schaub and K. Alfriend, "Impulsive Feedback Control to Establish Specific Mean Orbit Elements of Spacecraft Formations," *Journal of Guidance, Control, and Dynamics*, Vol. 24, July-August 2001, pp. 465–471.

[10] R. H. Battin, *An Introduction to the Mathematics and Methods of Astrodynamics*. 1801 Alexandar Bell Drive, Reston, VA 20191: American Institute of Aeronautics and Astronautics, Inc., revised ed., 1999.